Numerical analysis of the Albert Street station rock pillar

Jiwoo Ahn
BHP, Australia (formerly PSM)

ABSTRACT: This paper presents a case study on numerical analysis methods of hard rock pillars. The design of hard rock pillars is underpinned by experience in underground mining. However, such empirical methods were considered inappropriate for slender pillars with daylighting discontinuities such as the one encountered at Albert Street station for the Cross River Rail project in Australia. The imposed stresses were analysed using three-dimensional continuum finite different analysis. Numerical analyses using a discrete fracture network and the three-dimensional discrete element method was utilised to determine the confining stresses in terms of support required to maintain adequate stability against the imposed stresses. The analysis of the pillar was decoupled from the overall excavation for computational efficiency. The analyses indicated significant support requirements, resulting in the excavation of the rock pillar and replacement with mass concrete.

1 INTRODUCTION

Rock pillars are defined as in-situ rock that is left between adjacent underground openings. There is a wealth of experience and research in the design of pillars in underground mining, particularly in underground coal mines. According to Martin & Maybee (2000), hard-rock pillars have not received the same research attention partly due to the fewer mines that operate at depths sufficient to induce adequate stresses for failure, as well as the irregular geometries making it difficult to determine the loads. In either industry, pillars are commonly used to provide temporary and/or permanent support for large openings.

In civil tunnelling, rock pillars are typically confined in the longitudinal direction as they exist in-between twin tunnels. This confinement is removed on one side at cross-passages or Y-junctions, increasing stress concentrations as well as the risk of unfavorable structures daylighting. In some cases, the rock pillar is unconfined on all four sides, such as between twin adits.

Pillar designs are often completed using empirical methods. These methods are generally developed using existing case studies of stress induced failures in brittle rock and relate the pillar dimensions to a factored ratio of induced stress to rock strength. Therefore, such methods are not always appropriate for cases where the pillars include daylighting structures, as the capacity of the pillar in these cases are typically governed by the shear strength of the discontinuities and not the compressive strength of the rock mass. This makes slender pillars more unfavourable due to the higher daylighting probability of steeply dipping structures. In such cases, numerical analyses can be undertaken as presented by Thirukumaran et. al. (2017).

This paper presents the numerical analysis that was undertaken to assess the pillar strength in response to varying degrees of confinement, as well as to predict the induced stresses.

2 PROJECT

2.1 Background

Cross River Rail is a new 10.2-kilometre rail line from Dutton Park to Bowen Hills, which includes 5.9 kilometres of twin tunnels under the Brisbane River and CBD. The project includes construction of four new underground stations at Boggo Road, Woolloongabba, Albert Street and Roma Street. The station caverns are approximately 22 metres in span and 17 metres in height, with primary support typically comprising of rock bolts and a thin shotcrete layer.

At Albert Street station, a slender rock pillar is formed between the cavern and adjacent shaft as shown in Figure 1. Another pillar is formed on top between the two pedestrian adits, Figure 2. High stress concentrations were expected especially through the upper pillar due to arching stresses from the cavern and adits, as a result of the highly pre-loaded retention props.
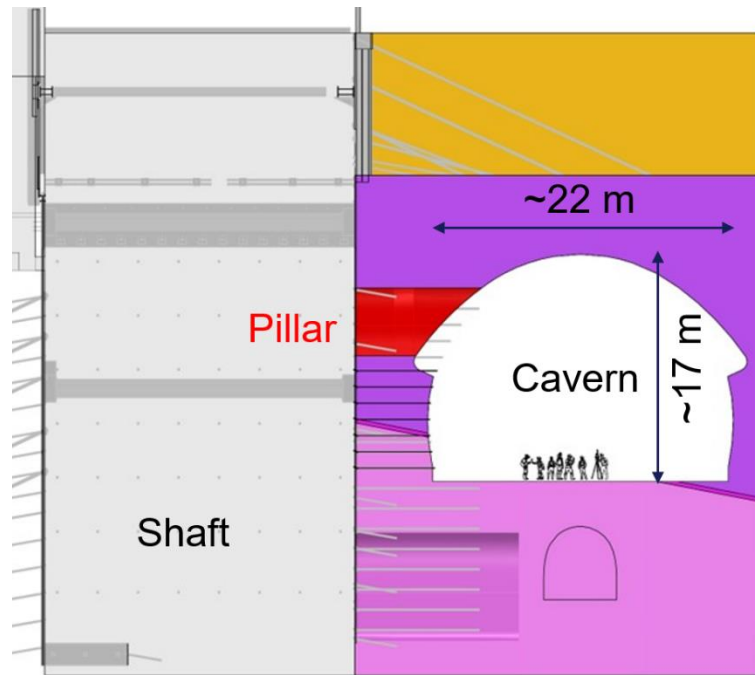
Figure 1. Section through Albert Street Station
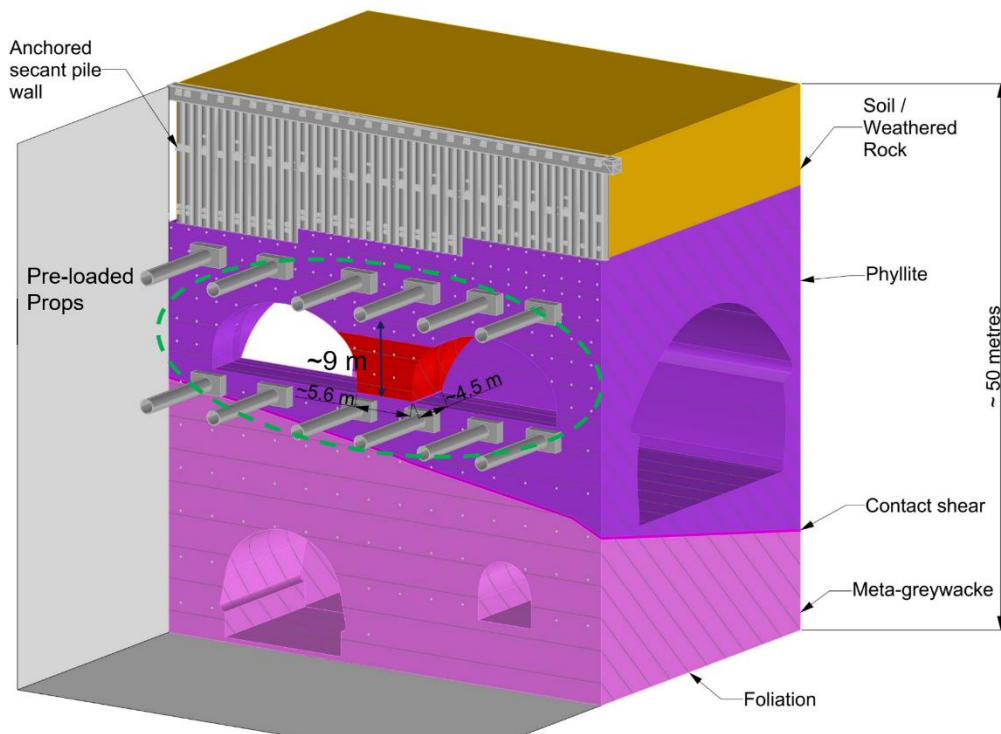
Figure 2. Isometric view of Albert Street Station

2.2 Geology

Albert Street station as well as much of the project is within the Neranleigh-Fernvale Group (NFG), a lithologically varied rock mass that largely comprises the basement rock of the Brisbane CBD. At Albert Street station, the lithologies are weakly metamorphosed sandstone (meta-greywacke) and phyllite. Foliation is present throughout the NFG but is particularly well developed in the phyllite dominated zones. Surface mapping and borehole imaging indicate that it is moderate to steeply dipping (typically 40 to 70°) to the northeast. However, both dip and dip direction vary throughout Brisbane because of

folding (Grubb, 1989). Although the foliation generally occurs as a fabric, defects do occur along it. These are generally tight, smooth to rough and without infill in fresh to slightly weathered rocks. In addition to foliation, two joint sets have been identified.

Figure 3. Typical fresh to slightly weathered NFG at Albert Street station from Cammack et. al (2022)

3 DISCRETE FRACTURE NETWORK

3.1 Introduction

A Discrete Fracture Network (DFN) is a stochastic method of fracture simulation (Tollenaar, 2008). A DFN represents the discontinuities within a rock mass as a cluster of fractures (Weir & Fowler, 2014a). It is a discontinuum method which provides a probabilistic, three-dimensional realisation of the non-deterministic fractures that constitute a rock mass. DFN models are a useful tool for visualisation and analysis of a rock mass (Weir & Fowler, 2014b). The application of DFNs for underground excavations have been explored by Starzec and Anderson (2002), Bakun-Mazor (2009), Menéndez-Díaz (2009) and Merrien-Soukatchof et al. (2011). Due to the stochasticity of the DFN's inputs, analyses can be readily undertaken on numerous DFN realisations. This allows for the probabilistic assessment of a design's robustness against unfavourable discontinuities.

3.2 Discontinuity Orientation

Discontinuity orientations from boreholes (geotechnical core logging and downhole imaging) shows the large variability of foliation. However, the boreholes are mostly "blind" to the sub-vertical jointing that were identified from mapping of outcrops and excavations. The two data sources were assessed in conjunction to determine the set statistics summarised in Table 1. Each discontinuity set has been characterised by its mean dip and dip direction, and Elliptical Fisher distribution coefficients on the basis of a Kolmogorov-Smirnov probability test. The Elliptical Fisher distributions allows for non-symmetrical variability in dip direction compared to dip angle, with the addition of a second Fisher coefficient and the major axis direction.

| a) Downhole televiewer | b) Mapping |
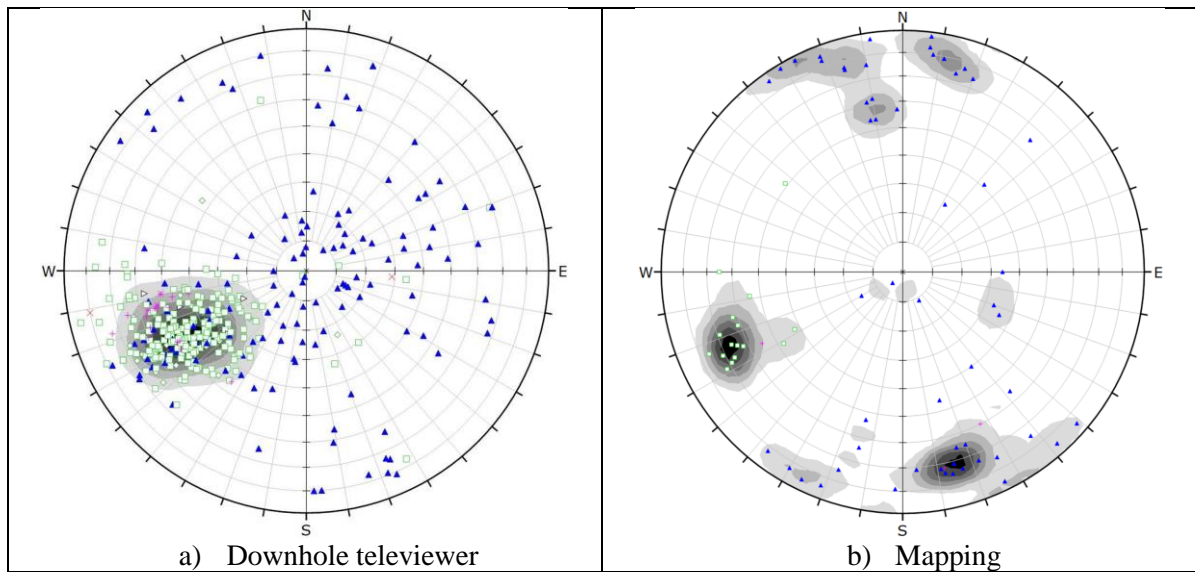
Figure 4. Stereonet of discontinuity orientations

Table 1. Summary of discontinuity set orientation statistics.

Parameter	Foliation	Joint 1	Joint 2
Mean dip & dip direction	47°/062°	38°/247°	86°/316°
Fisher coefficient (K1/K2)	29.4/1.5	9.6/1.3	18.2/1.2
Major axis trend & plunge	083°/046°	305°/22°	234°/73°

3.3 Discontinuity Size

Fracture size is typically the most difficult parameter to quantify, particularly from borehole datasets. Some studies have relied upon published fracture lengths for the same lithology at different sites (Weir et al., 2014), while others have estimated size using empirical relationship between fracture length and aperture for similar rock types (e.g. Starzec and Andersson, 2002). The intersection of a fracture with a mapping surface forms a one-dimensional trace. It has been found that the distribution of trace lengths will follow a log-normal distribution (Dershowitz & Einstein, 1988).

Trace lengths from mapping have been used for informing the fracture size distributions. The trace lengths are well described by a lognormal distribution, as shown by the similarity in the cumulative frequency curve and the fitted log-normal distribution, Figure 5.

| a) Foliation | b) Joint 1 | c) Joint 2 |
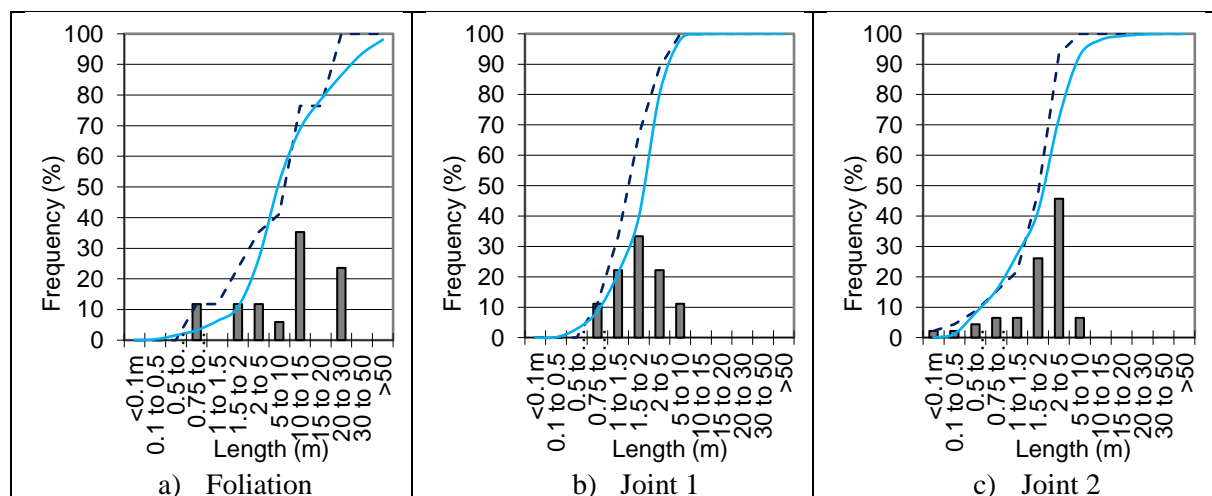
Figure 5. Histogram and cumulative frequency of mapped trace lengths

Table 2. Summary of discontinuity set trace length distributions.

Parameter	Foliation	Joint 1	Joint 2
Mean	11.5	2.6	2.7
Standard Deviation	8.7	2.0	1.7

3.4 Spatial Distribution

The spatial distribution of fractures is typically estimated from spacing measurements along sampling lines such as boreholes. Box dimension analysis were undertaken, which involves subdividing the boreholes into boxes of varying sizes and counting the number of boxes containing discontinuities (Weir & Fowler, 2016). If the slope of this line is near horizontal, then the fractures can be considered to be distributed according to a Poisson process. Based on this analysis, the Enhanced Baecher model, which is a random spatial distribution model that is based on a Poisson process (Dershowitz, et al., 2015), was adopted for each defect set.

3.5 Discontinuity Intensity

The intensity controls the number of discontinuities that are generated in the DFN. It can be quantified using several methods depending on available data sources. For this study the number of fractures per unit length of borehole or scanline (P10) was adopted to control fracture intensity. Discontinuities are generated in the DFN until the number of intersected discontinuities at the borehole or scanline reaches the defined P10 value.

The P10 values of each borehole and scanline were calculated and are summarised in Table 4. Borehole lengths with no imaging or poor-quality imaging were excluded from the P10 calculation. The boreholes exhibit significant variance in measured fracture intensities across the Albert Street station site. Therefore, only the borehole closest to the pillar was used for calibrating the intensity of the DFN.

As previously discussed, the vertical boreholes are likely to under-sample the sub-vertical joint set. Therefore, the intensity of Joint 2 has been calibrated using the mapping scanlines, and the other two sets against the boreholes. The proportion of the total P10 value that is attributed to each discontinuity set is summarised in Table 5.

Table 3 – Fracture Intensity Terminology (after Dershowitz and Herda, 1992)

		Dimension of Measurement				
		0	1	2	3	
Dimension of Sample	1	P_{10} No. of fractures per unit length of borehole	P_{11} Length of fractures per unit length			Linear Measures
	2	P_{20} No. of Fractures per unit area	P_{21} Length of fractures per unit area	P_{22} Area of fractures per unit area		Areal Measures
	3	P_{30} No. of Fractures per unit volume		P_{32} Area of fractures per unit volume	P_{33} Volume of fractures per unit volume	Volumetric Measures
		Density		Intensity	Porosity	

Table 4. Summary of total P10 values by data source

Parameter	Boreholes	Mapping
Number	8	3
Mean	1.8	1.9
Range	0.5 – 2.7	1.3 – 1.9

Table 5. Proportion of total P10 of each discontinuity set

Parameter	Foliation	Joint 1	Joint 2
P10 Proportion (Boreholes)	74%	22%	-
P10 Proportion (Mapping	-	-	65%

3.6 Fracture Generation

The discrete fracture network was generated using Fracman. A detailed methodology for the construction of a DFN is provided by several authors, including Dershowitz et al. (2015), Starzec and Anderson (2002) and Weir and Fowler (2014b).

The generation region for the fracture network was a rectangular prism, with approximate dimensions of 500 metres x 320 metres x 50 metres. The generation volume exceeded the volume required for stability simulations but was kept large to minimise edge effects. Figure 6 shows an oblique view of the generation region. Actual borehole intercepts were used to directly control fracture intensity until the P10 values from the generated fractures matched that of the boreholes and mapping traverses. Representative fracture sizes were generated according to lognormal distributions. The generation region was then populated with fractures until the average P10 across the borehole and scanlines were achieved.

The DFN was validated by comparing the statistical distribution of the outputs with the inputs. In addition, visual evaluation was undertaken to check that the DFN "makes sense" from a geological perspective and that variables such as length and intensity are as expected based on the inputs. For example, the DFN has been intersected with an existing NFG outcrop for visual confirmation that the DFN has created a reasonable representation, Figure 7. The fracture network was generated 100 times. The number of fractures and the P32 values from each DFN realisation are plotted, along with the rolling average.

The P32 values from each DFN realisation are shown alongside the rolling average in Figure 8. The P32 value provides a "true" measure of the intensity and can be readily be used as an input for DFN generation in other packages.

a) boreholes and scanlines for calibrating intensity   b) Example DFN with Foliation (green), Joint 1 (magenta) and Joint 2 (blue)
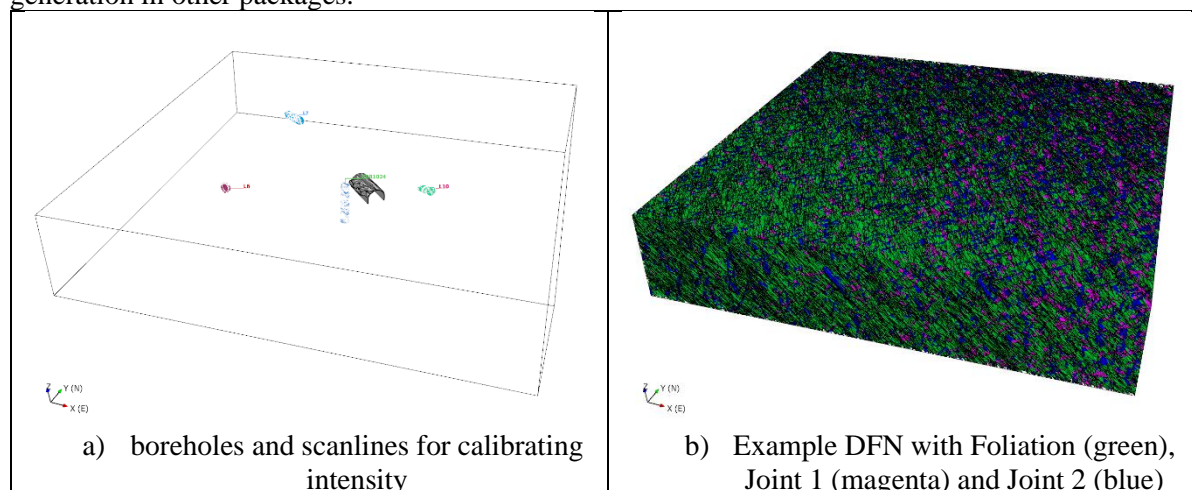
Figure 6. DFN Fracture generation region
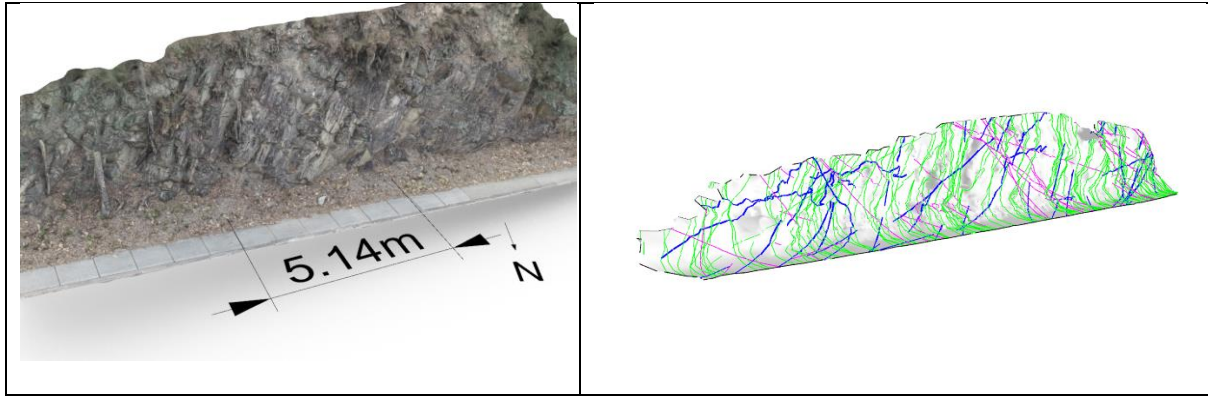
Figure 7. Tracemap of DFN intersected with outcrop
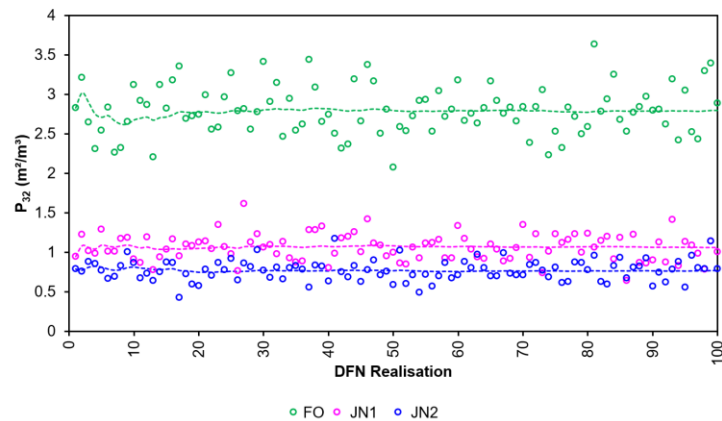
Figure 8. Rolling average of P32 values over 100 DFN realizations.

4 NUMERICAL ANALYSIS

4.1 Pillar strength

3D numerical analyses of the Albert Street pillar were undertaken using the commercial distinct element method software 3DEC. The irregular pillar geometry was approximated as a rectangular prism with 5.2 metre width x 6.4 metre length x 9.1 metre height dimensions. Discontinuities were generated using the DFN parameters presented in Section 3 and modelled as linear force-displacement spring relation with a Mohr-Coulomb frictional strength envelope. The blocks bound by these discontinuities were modelled as linearly isotropic, elastic material with a generalised Hoek-Brown strength envelope and an appropriately assessed GSI value.

The Albert Street pillar was modelled in isolation at varying confining pressures to simulate ground support. The pillar was then loaded by applying an axial stress at the top. Failure was inferred by interpreting the calculated stress-strain curve of each test, effectively simulating a large-scale triaxial test, Figure 9. This methodology is consistent with that of Thirukumaran et. al. (2017) and Kineti et. al. (2021). This approach has significant benefits over a traditional synthetic rock mass approach such as that presented by Mas Ivars et. al. (2011) as it requires significantly less input parameters, the input parameters can more readily be assessed, and is more computationally efficient.

For each confining stress, the simulation was run with 10 DFN realisations, returning a significant spread in the maximum axial stress prior to failure. Because the pillar typically had at least one persistent defect that daylighted on all four sides, the strength of the pillar at zero confinement was typically zero. At higher confining stresses, the failure appeared to change from a brittle sliding to a more ductile crushing type mechanism. The pillar strength was insensitive to varying rock mass strengths and stiffnesses. However, the results were highly sensitive to the shear strength of the discontinuities. An increase in friction angle by just 5° resulted in a significant increase in pillar strength as shown in Figure 11, confirming that the pillar is largely governed by the discontinuities.

Table 6. NFG rock mass parameters

γ (kN/m³)	UCS (MPa)	Ei (GPa)	v	mi
27	30	12	0.2	15

Table 7. Discontinuity parameters

Type	c'	φ' (°)	kn (MPa/m)	ks (MPa/m)
Foliation	0	35	10000	1000
Joints	0	30	10000	1000
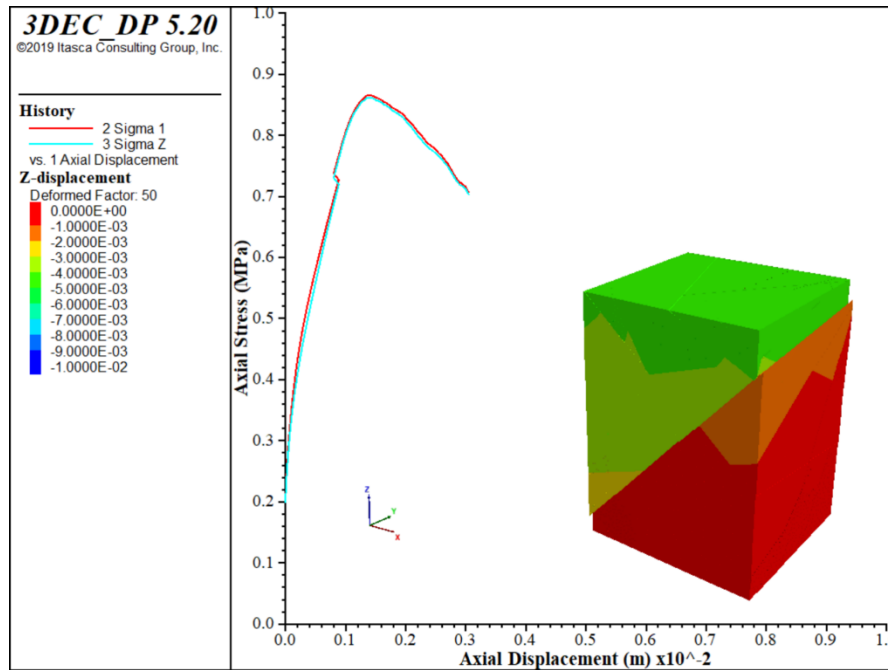
Figure 9. Example simulated stress strain curve

| a)   Low confining stress | b)   High confining stress |
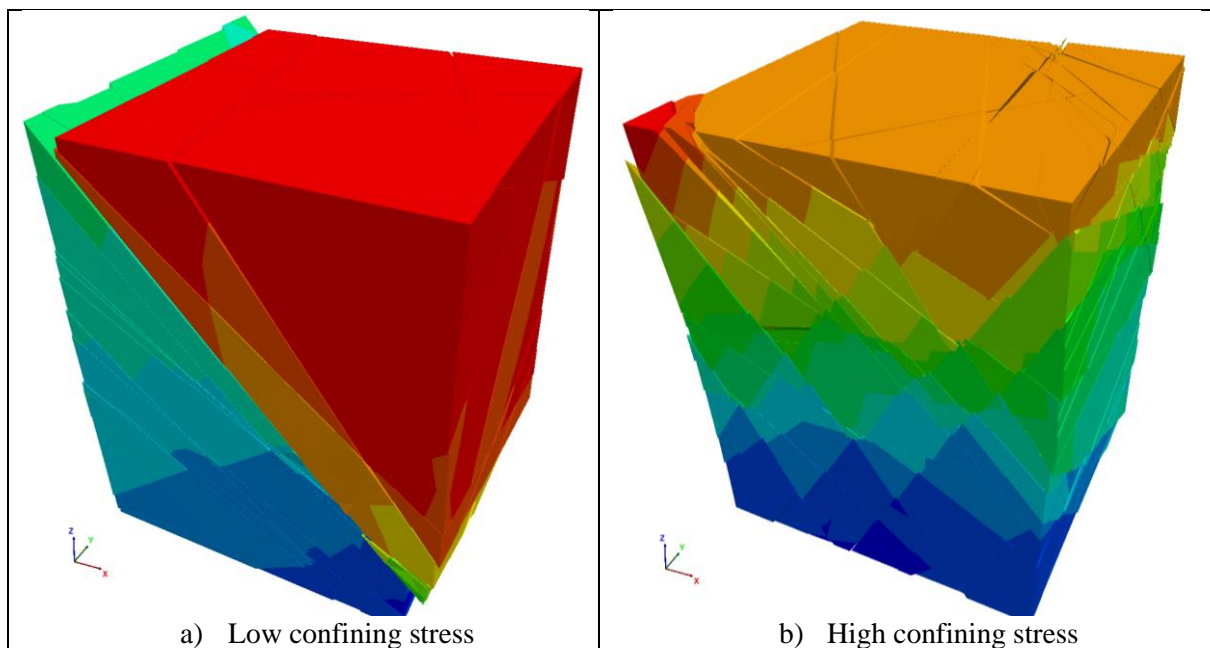
Figure 10.Pillar failure mechanisms
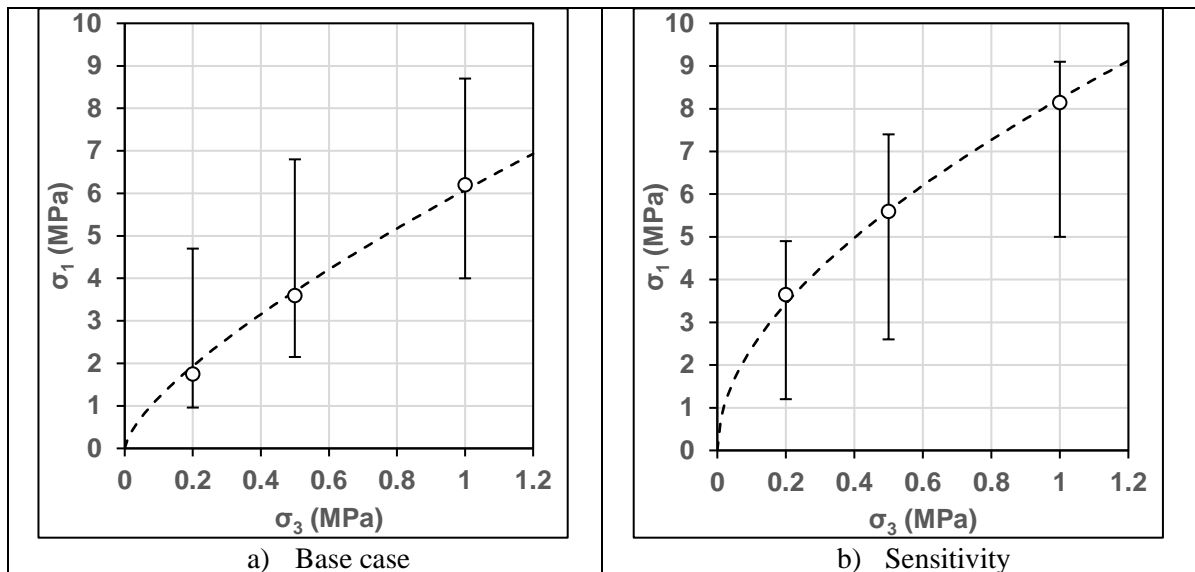
Figure 11. Pillar strength envelopes

4.2 *Concrete replacement*

3D continuum stress-deformation analysis was undertaken of Albert Street station using Flac3D, in order to assess the induced stresses on the pillar. The shaft, cavern, and adits were all modelled as per the expected construction sequence. For an in-situ stress ratio of 2, which was considered to represent the base case, stresses of between 2 and 5 MPa were calculated on the pillar, requiring up to about 800 kPa of confining stress according to the assessed pillar strength envelope, even before any safety factors are applied. For comparison, the empirical pillar strength formulae summarised by Martin & Maybee (2000) indicates that for a width to height ratio of about 0.5, the ratio of pillar strength to UCS ranges between 0.2 and 0.3, or about 6 to 9 MPa for the NFG.

To provide such confinement, high strength bolts at very close spacing would be required. In addition, the bolts required high pre-stressing to limit the pillar deformations required to mobilise the confining stresses. In addition, this design would have significant implications on the excavation and support sequence. Ultimately, the pillar was not left in-situ but instead excavated and replaced with concrete prior to the excavation of the adits or the adjacent shaft, eliminating the risk of structurally controlled failure.
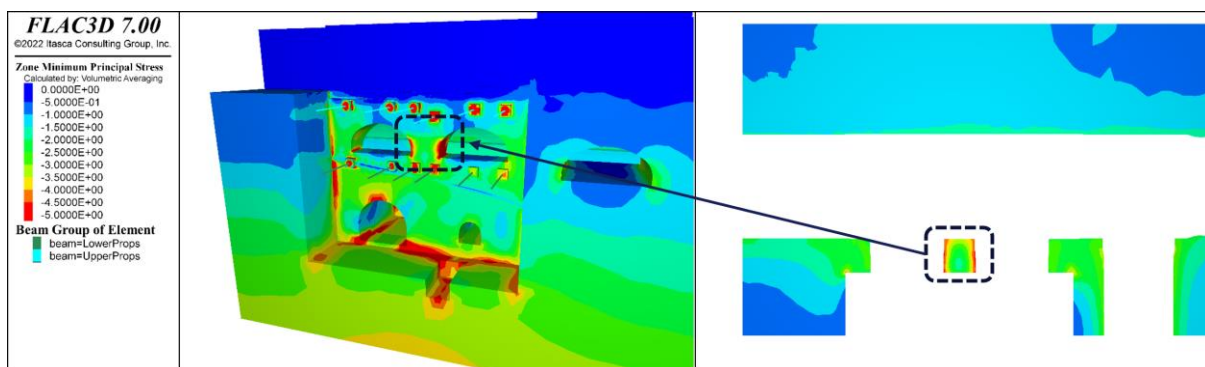
Figure 12. Example simulated stress strain curve

| a) View of pillar excavation from inside the cavern | b) View of the completed concrete replacement from the shaft |
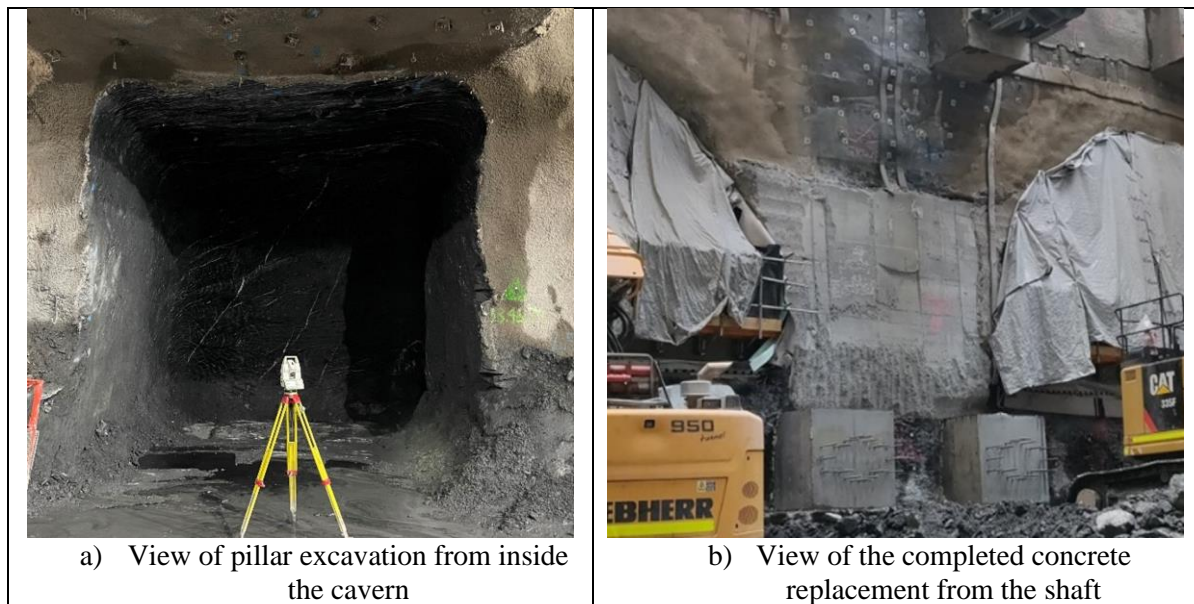
Figure 13. Concrete pillar replacement

5 CONCLUSION

This paper presents a case study on assessing the strength of a rock pillar. Due to the slenderness of the pillar as well as the discontinuities present in the foliated rock mass, empirical methods from hard rock mining experience were found to be inappropriate. Numerical analysis was undertaken using the 3D distinct element method alongside a calibrated discrete fracture network to simulate large scale triaxial tests on the pillar. Based on the calculated induced stresses on the pillar, significant ground support requirements were assessed. Ultimately, the rock pillar was removed and replaced with concrete, removing the need for onerous limits on excavation and support sequencing, as well as any risks due to geological and geotechnical uncertainty.

ACKNOWLEDGEMENTS

REFERENCES

Bakun-Mazor, D., Hatzor, Y. H., & Dershowitz, W. S. (2009). Modelling mechanical layering effects on stability of underground openings in jointed sedimentary rocks. *International Journal of Rock Mechanics and Mining Sciences*, 262-271.

Cammack, R., Bertuzzi, R., Smith, A., & Brehaut, R. (2022). Rock Mass Parameters For The Brisbane CBD. *Australian Geomechanics Journal, 57*(4).

Dershowitz, W. S., & Einstein, H. H. (1988). Characterizing rock joint geometry with joint system models. *Rock Mechanics and Rock Engineering 21, no. 1*, 21-51.

Dershowitz, W. S., Lee, G., Geier, J., Foxford, T., La Pointe, P., & Thomas, A. (2015). *Fracman - Interactive Discrete Fracture Data Analysis, Geometric Modelling, and Exploration Simulation, user documentation, version 7.5.* Golder Associates.

Grubb, B. K. (1989). *Engineering geology of the central business district of Brisbane.* Queensland University of Technology.

Hutchinson, D. J., & Diederichs, M. S. (1996). *Cablebolting in underground mines.* Bitech Publishers Ltd.

Keneti, A., Pouragha, M., & Sainsbury, B.-A. (2021). Review of design parameters for discontinuous numerical modelling of excavations in the Hawkesbury Sandstone. *Engineering Geology, 288.*

Martin, C. D., & Maybee, W. G. (2000). The strength of hard-rock pillars. *International Journal of Rock Mechanics & Mining Sciences, 37*(8), 1239-1246.

Mas Ivars, D., Pierce, M. E., Darcel, C., Reyes-Montes, J., Potyondy, D. O., & Cundall, P. A. (2011). The synthetic rock mass approach for jointed rock mass modelling. *International Journal of Rock Mechanics and Mining Sciences, 48*(2), 219-244.

Menendez-Diaz, A., Gonzalez-Palacio, C., Alvarez-Vigil, A. E., & Gonzalez-Nicieza, C. (2011). Analysis of tetrahedral and pentahedral key blocks in underground excavations. *Computers and Geotechnics*, 1009-1023.

Merrien-Soukatchoff, V., Korini, T., & Thoraval, A. (2011). Use of an integrated discrete fracture network code for stochasic stability analyses of fracture rock masses. *Rock Mechanics and Rock Engineering*, 159-181.

Starzec, P., & Anderson, J. (2002). Probabilistic predictions regarding key blocks using stochastic discrete fracture networks - examples from a rock cavern in south-east Sweden. *Bulletin of Engineering Geology and the Environment*, 363-378.

Thirukumaran, S., Oliveira, D., & Asche, H. (2017). Numerical study of rock pillars for large span tunnels in Hawkesbury sandstone. *16th Australasian Tunnelling Conference 2017: Challenging Underground Space : Bigger, Better, More* (pp. 920-929). Sydney: Engineers Australia.

Tollenaar, R. (2008). *Characterisation of discrete fracture networks and their influence on caveability and fragmentation, MASc thesis.* Vancouver, BC.: The University of British Columbia.

Weir, F. M., & Fowler, M. (2014a). Application of DFN Modelling to Large Open Pit Slope Design in Australia. *DFNE 2014, 1st International Conference on Discrete Fracture Network Engineering*.

Weir, F. M., & Fowler, M. (2014b). An Introduction to Discrete Fracture Network Modelling and its Geotechnical Applications. *AUSROCK 2014: Third Australasian Ground Control in Mining Conference, =.*

Weir, F. M., & Fowler, M. J. (2016). Discrete fracture network modelling for hard rock slopes. *Proceedings of the First Asia Pacific Slope Stability in Mining Conference* (pp. 157-168). Perth: Australian Centre for Geomechanics.